Spatially forced corotating Taylor-Couette flow

Eliko Ikeda and Tony Maxworthy

Department of Aerospace Engineering, University of Southern California, Los Angeles, California 90089-1191

The response of a flow to which an external control force is applied is of great general interest. The flow studied was a variation of classical circular Taylor-Couette flow in that it was spatially forced by sinusoidal modulations on the inner cylinder, with a forcing wavelength incommensurate with the natural length scale of the Taylor vortices. It was found that this forcing did not affect the conditions for the onset of the vortices, but it did fix the size of the vortices. For the conditions of geometry and flow variations used here, the natural wavelength did not seem to appear in this system. Many of the complex states observed in the unforced case were observed also in the forced case. However, two new types were observed in the present case. They both involved irregularities of the vortices, and they occurred at slow and fast rotation rates, and were named unstable irregularities and temporal irregularities, respectively. The unstable irregularities occurred throughout the entire tank and were constantly changing. The temporal irregularities occurred locally and would appear only for brief periods of time. The azimuthal rotation rate of the irregularities was proportional to the average rotation rate of the cylinders.

PACS number(s): 47.20.$-$k, 47.32.$-$y

INTRODUCTION

Simple patterns of many types of flows are stable and can be sustained until a critical value of a control parameter is reached, at which point infinitesimal perturbations grow and the flow becomes unstable. The instability which develops is often a transition from a simple to a more complex laminar state and eventually can result in transition to a fully turbulent state, as the control parameter is increased. In the present case, in an effort to understand the flow and how it can be controlled, an external perturbation was applied, and the response of the flow was studied.

Many studies, both theoretical and experimental, have been performed on Taylor-Couette flow, the flow in the annular gap between two concentric, independently rotating cylinders. The symmetries in the flow lend themselves to theoretical studies [1–3], while the distinct transitions in the flow to a more complex state break the symmetry in the flow and, thus, can be studied as a dynamical system with bifurcations [4]. Also, Taylor-Couette flow may be easily constructed for detailed experimental studies [1,5]. A series of stable states, which can be easily visualized, occurs between the laminar and turbulent states. The study of vortex flow is of interest because vortical structures are present in turbulence and these structures determine the characteristic scales. In order to control the scales in turbulence, an understanding of how to control the scales of the vortices is needed. In this experiment, an external force was applied through a wavy boundary. The wavelength of the forcing was incommensurate with the natural wavelength, which is given by twice the gap width of the two cylinders, in order to study the effect on the length scales and the transitions of Taylor vortices.

EXPERIMENTAL APPARATUS

Taylor-Couette flow was established in the annular gap between two concentric, rotating Plexiglas cylinders (Fig. 1). The outer cylinder had a radius, R_2 of 13.94 ± 0.01

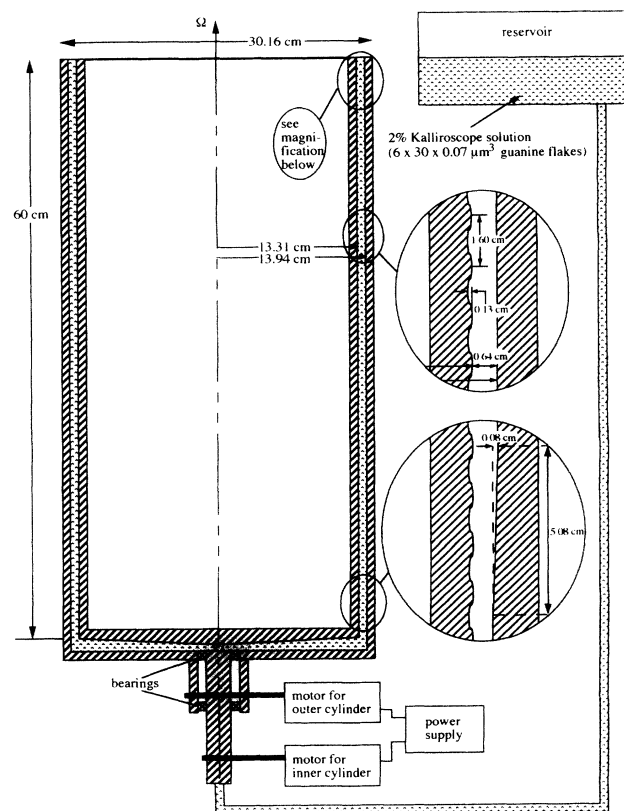
FIG. 1. Experimental apparatus.

cm and the test section was 49.85±0.01 cm long. At the top and bottom of the cylinder, 5.08-cm extensions were added which tapered inward toward the test section by 0.076 cm in order to allow for a continuous vortex pair wavelength adjustment in the test section. Riecke [6] theoretically observed that this spatially ramped end condition reduced the accessible wavelengths compared with the unramped case in which the wavelength depended on the length of the section. Also, experimental studies have been done with ramped sections at one end of the test section, such as that by Ning, Ahlers, and Cannell [7] with the same results, but no studies have been done with ramped sections at both ends. Their results were used to design the apparatus, but ramped Taylor-Couette flow was not the focus of our study. The inner cylinder contributed the forcing for the system, in the form of sine wave modulations along the length of the cylinder. The average radius of the inner cylinder, R_1, was 13.37±0.01 cm, for an $\eta = R_1/R_2 = 0.959$. The amplitude of the modulations was ±0.064 cm, which was 10% of the minimum gap width. The wavelength of the modulations was 1.60 cm, which was 126% of twice the minimum gap width (the wavelength of an unforced vortex pair). The length of the test section would allow for 31 forced wavelength vortex pairs or about 44 unforced wavelength vortex pairs. Both cylinders rotate independently by two Glentek Model GM4020 feedback controlled dc motors, which were, in turn, controlled by a Macintosh computer. The rotation period of the cylinders was measured visually, using a stopwatch, with a resultant accuracy in the rotation period of ±0.2 s.

The annular gap was filled with tap water and the flow was visualized by the addition of 2% by volume Kalliroscope solution, which consisted of guanine flakes [8] of dimensions approximately $6 \times 30 \times 0.07$ μm^3. At this concentration, the viscosity of the water increased by only 1%. These anisotropic flakes were used to visualize the flow since they spend more time aligned with the shear of the flow than they spend rotating. These reflective flakes are almost neutrally buoyant. With no flow, they tend to settle in about 24 h. In laminar flow, the flakes in the gap width align with the shear such that the wavy modulations on the inner cylinder can barely be seen through the field of particles. There was no tendency for the corrugations to generate a secondary flow before the Taylor instability boundary was reached. Flow regimes were determined visually, and wavelengths were measured from 35-mm still photographs.

Significant parameters for the experiment include the inner cylinder and outer cylinder Reynolds numbers, Re$_i$ and Re$_o$, respectively, given by

$$\text{Re}_i = \frac{\Omega_1 R_1 d}{\nu} \quad \text{and} \quad \text{Re}_o = \frac{\Omega_2 R_2 d}{\nu} , \tag{1}$$

where Ω_1 and Ω_2 are the rotation rate of the inner and outer cylinders, d is the average gap width, and ν is the viscosity of the fluid. In this experiment, ν is 0.01 cm^2/s. The viscous time scale for this flow depended on the average gap width and was given by

$$\tau \sim \frac{d^2}{\nu} = 49 \text{ s .} \tag{2}$$

All studies were done in the corotating case with the final rotation rate reached by quasisteady increases in rotation rate. This was achieved by increasing the Reynolds number in steps of 50 in a fraction of a second. Then the flow was allowed to stabilize for about five viscous time scales.

RESULTS

1. Stability boundary

The onset of Taylor vortices (Fig. 2) was determined by two methods. With the first method, the outer cylinder rotation rate was set first. At any outer Reynolds number, the resulting flow would be the stable Couette flow, parallel shear flow between two rotating cylinders. Then the inner cylinder rotation rate was increased quasisteadily, until the boundaries of the Taylor vortices were observed visually. This was repeated for various fixed outer Reynolds numbers and the onset is indicated in Fig. 2 by the " + " symbol. With the second method, the inner
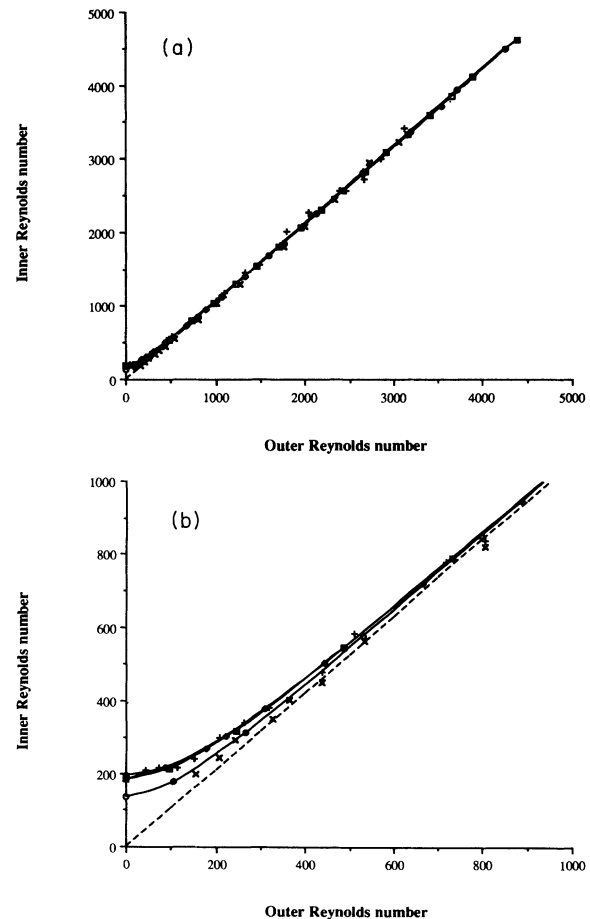

FIG. 2. (a) Stability diagram: − − −, Rayleigh's criterion; Taylor's theory, □ average gap width; ◆, minimum gap width; ○, maximum gap width; ■, Chandrasekhar, forced wavelength; experimental results, +, vortices appear; ×, no vortices. (b) Enlargement of stability diagram at lower Reynolds numbers.

cylinder rotation was first set to the final desired rotation rate while the outer cylinder was stationary. In this case, the flow can become unstable, and depending on the inner Reynolds number, various flow regimes can occur, as will be detailed in the following subsection. Then the outer Reynolds number was increased, thus passing through various flow regimes, until there was no vortical motion and the flow had become Coutette flow. This was also repeated for various fixed inner Reynolds numbers and is shown in Fig. 2 as the "×" symbol. There was a shift in the two results, with the second method resulting in a lower critical Reynolds number. This may be due to a hysteresis effect, that is, once the vortices form, a lower rotation rate is required for them to decay. Though Park, Crawford and Donnelley [9] observed that there is no hysteresis if the rate of change in the rotation rate is small enough, their study was done with the outer cylinder at rest. The absence of hysteresis was observed when both increasing and decreasing the inner Reynolds number. In our study, the rate of change in rotation rate was not small enough to have the absence of hysteresis. Also, our inner Reynolds number was not decreased to reach a final rotation rate. Rather, the outer cylinder Reynolds number was increased until the flow was no longer unstable. Another factor that may result in a shift in the data is that, to determine the stability boundary, steps of outer Reynolds number of about 50 were taken and, thus, the scatter in the data might not be as large if smaller steps were taken. For large Reynolds numbers, the data followed the theory by Taylor [1]. The scatter was probably due to the difficulty in visualizing the vortices since at onset, there was only slight vortical motion. In determining the correct parameters to use in the theory, the results of using either the minimum, the average, or the maximum gap width were found to be almost identical, except at small Reynolds number, where the instability occurred at a lower Reynolds number for the maximum gap width case, as observed by Taylor. The data where the outer Reynolds number was fixed and the inner Reynolds number was increased seem to follow the average and the maximum gap width case, but the data determined by the second method were closer to the minimum gap case. Taylor [1] determined that the larger the gap width, the lower the Reynolds number required for the instability to develop; thus, it was expected that the maximum gap width would initiate the production of the vortices. Hence, it may be that the minimum gap width would be the dominant factor in scaling the disappearance of the vortices. The inviscid theory by Rayleigh [10], as well as the viscous theory of Chandrasekhar [2], in which the disturbance wavelength was a variable, were plotted also. The wavelength used in Chandrasekhar's theory for Fig. 2 was the forced wavelength. The result was also very similar to the previous cases for large Reynolds numbers, and to the minimum gap width case for small Reynolds numbers. But the effect of the forcing was negligible on the stability boundary.

The wavelength at onset was always equal to the forcing wavelength, as was also observed by Koschmieder [11]. Even with the ramped end sections which would result in a constraint leading to wavelengths at or near the
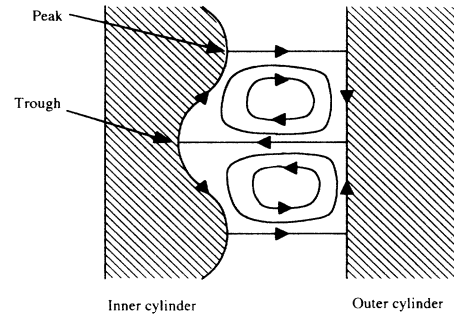

FIG. 3. Sketch of a cross section of Taylor vortex flow with a modulated boundary.

natural wavelength [6,7], only the forced wavelength was observed. It does not seem possible to obtain the natural wavelength in this system, most probably because the 10% amplitude modulation of the forcing was too great. It is not known at what level of forcing it would cease to dominate the flow and we would find the types of commensurate-incommensurate behavior we originally hoped to find. The outflow of the vortex pair always occurred at the peak of the sine wave modulations, i.e., at the minimum gap width, because the centrifugal force on a particle was larger at the peaks than at the troughs of the modulations of the inner cylinder, (Fig. 3). Since the external forcing dominated the size of the vortices and only the forced wavelength appears in the system, the number of vortex pairs in the system remained constant, whereas, in the unforced case, the number of vortex pairs in a system depended on the flow conditions [5].

2. Flow regimes at supercritical Reynolds numbers

At Reynolds numbers above the stability boundary, the flow regimes observed were compared with the unforced case, as studied by Andereck, Dickman, and Swinney [12], Andereck, Liu, and Swinney [13], and Baxter and Andereck [14]. The same two methods used to determine the stability boundary were used to determine the boundaries of the various regimes. Since many regimes were observed, two separate plots are presented here.

In Fig. 4 the regimes observed were also found by Andereck et al. [12,13] for the unforced case. Thus, just above the stability curve, at low outer Reynolds numbers, $Re_0 < 1500$, the boundary of the vortices became wavy. First, the outflow boundary became unstable to a wavy perturbation, while the inflow boundary remained straight. At higher values of the inner Reynolds numbers, both boundaries became unstable. Generally, these flow regimes occur at similar locations on a plot of onset versus inner and outer Reynolds number, as in the unforced case, and the waviness appears to have the same origin in the shear layers generated by the secondary flow. Since the velocity of the waves was not measured, the difference between wavy vortex flow and wavelets and modulated wavy vortices as discussed in Andereck, Dickman, and Swinney [12] could not be distinguished. However, we note that the wavy inflow, straight outflow case
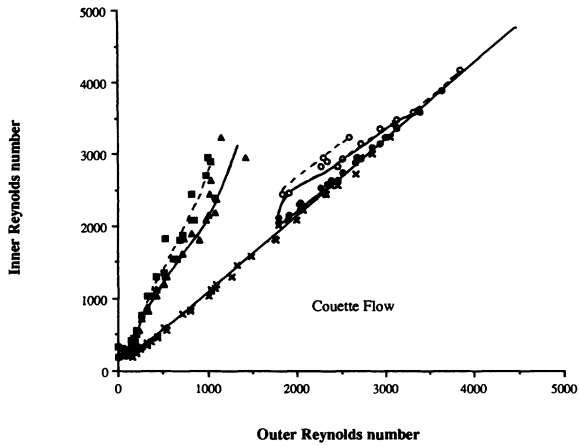
FIG. 4. Flow regimes: ——, Taylor's theory, average gap width; ×, Taylor vortex flow; ▲, wavy outflow and straight inflow; ■, wavy outflow and wavy inflow; ●, twists; ○, wavy twists.

was not observed in the forced case. In general, the outflow boundary seems to be more unstable than the inflow boundary.

Twists and wavy twists were also observed in the forced case. As in the unforced case, twists occurred at higher outer Reynolds number, just above the stability curve, with wavy twists occurring at higher inner Reynolds number. But there was not an overlap of twist and wavy vortices for a given outer Reynolds number as in Andereck, et al. [12,13]. This could be due to our smaller gap width, which delays transitions to instabilities. Though turbulent vortex flow was observed, it was a gradual transition, and thus, the exact boundaries of turbulent vortex flow could not be determined accurately.

In Fig. 5 the two new regimes, which were not observed in the unforced case, were mapped. They were two distinct types of irregularities of the vortices and
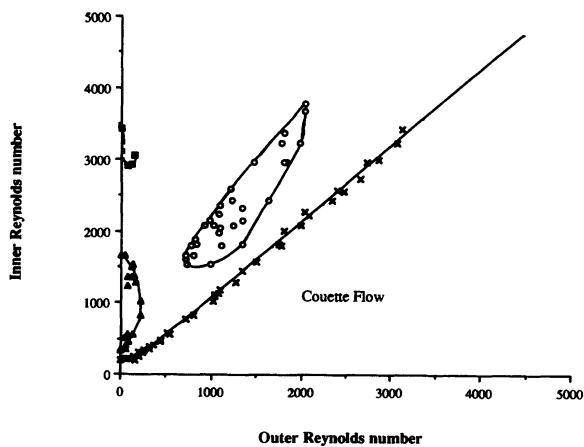

FIG. 5. Flow regimes, continued: ——, Taylor's theory, average gap width; ×, Taylor vortex flow; ▲, unstable irregularities; ■, large vortex; ○, temporal irregularities.

were named "unstable irregularity" and "temporal irregularity," while they occurred at slow and faster outer cylinder rotation rates, respectively. The unstable irregularity [Fig. 6(a)] developed from the wavy vortices. As the inner Reynolds number was increased, the amplitude of the waves on the vortices increased to a point where they broke and irregularities occurred. These irregularities were continually moving and changing in time and, thus, were not like the braid vortices observed by Andereck, Dickman, and Swinney [12]. These irregularities appeared throughout the entire tank. Upon increasing the inner Reynolds number further, the irregularities disappeared and wavy Taylor vortex flow was almost fully recovered, except at random locations throughout the tank where vortices did not appear. The flow at these locations appeared to be only in the azimuthal direction. Upon increasing the inner Reynolds number, the vortices next to these regions began to grow and became a vortex pair of twice the wavelength of the surrounding vortices. The nonuniformity in vortex size had the appearance of the nonuniformity observed by Baxter and Andereck [14] for the unforced case. The two cases are similar in that these large vortices were not transients, they did not occur at the same location in the tank for every run, and the appearance of the large vortices was hysteretic. As in the unforced case, once the large vortices were formed,
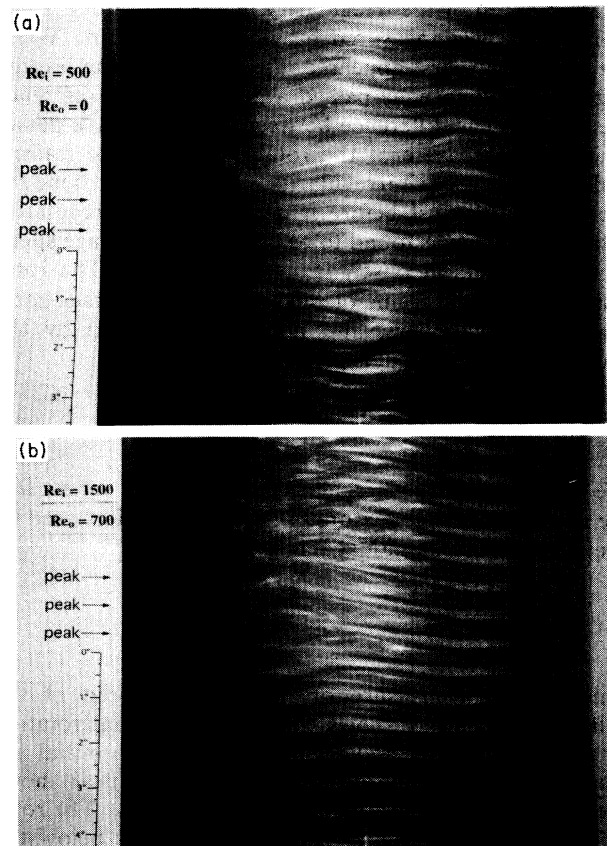

FIG. 6. (a) Photograph of unstable irregularities. Flow is from left to right. $Re_i = 500$, $Re_o = 0$. (b) Photograph of temporal irregularities. Flow is from left to right. $Re_i = 1500$, $Re_o = 700$.

they persisted. However, the large vortices in the unforced case occurred at higher outer Reynolds numbers and were not observed at an outer Reynolds number of zero (where they appeared in the present case). Also, in the unforced case, there was no development of the large vortices from a region of purely azimuthal flow.

At higher outer rotation rates, temporal irregularities occurred [Fig. 6(b)]. These irregularities appeared locally and usually moved vertically (either up or down) in the tank and were initially of the form of a bulge in the vortices. This bulge would sometimes grow and the vortices would break and reconnect with an adjacent vortex of the same direction. Some irregularities affected only a few vortex pairs, others affected the entire length of vortex pairs, but the irregularities never spread around the circumference of the tank. The irregularities could exist for a period of two average cylinder rotations or they could exist for over 200 average cylinder rotations. There could be more than one irregularity at a given time, and there could be some time when there were no irregularities at all.

3. Characteristics of temporal irregularities

One of the flow regimes which was a result of the forcing was the temporal irregularities. This was studied in more detail to understand the effect of the spatial forcing on the Taylor vortices at supercritical rotation rates. The rotation speed of the irregularity in the laboratory frame of reference was measured by videotaping them. When the irregularity first appeared, the time when the leading edge and trailing edge passed a given point of reference was noted. The difference between two successive passes would be a measure of the rotation rate of the leading and the trailing edge irregularity. This was also done for the irregularity just before it decayed. The irregularity rotation rate ω was found to be close to the average speed of the cylinders at onset, $\Omega_{ave}=(\Omega_1+\Omega_2)/2$. The rotation speed, in the frame of reference of the average rotation of the cylinders, and nondimensionalized by the average rotation speed, is given by

$$\omega'=\frac{\omega-\Omega_{ave}}{\Omega_{ave}} . \tag{3}$$

We chose to plot the irregularity rotation rate versus Ω_C, the nondimensional measure of the Coriolis effect used by Weisshaar, Busse, and Nagata [15], defined as

$$\Omega_C=\frac{(\Omega_1+\Omega_2)d^2}{\nu} . \tag{4}$$

This is also a measure of the average speed of the cylinders. Figure 7 shows the nondimensional rotation rates of the leading and trailing edges at the initial appearance of the temporal irregularities and Fig. 8 shows the same quantities just before it finally decays. The rotation rate of the irregularity was just slightly below the average rotation rate. At its initial appearance, the leading edge was consistently faster than the trailing edge. This resulted in the growth of the irregularity in its azimuthal length. Just before it decayed, the speed of the
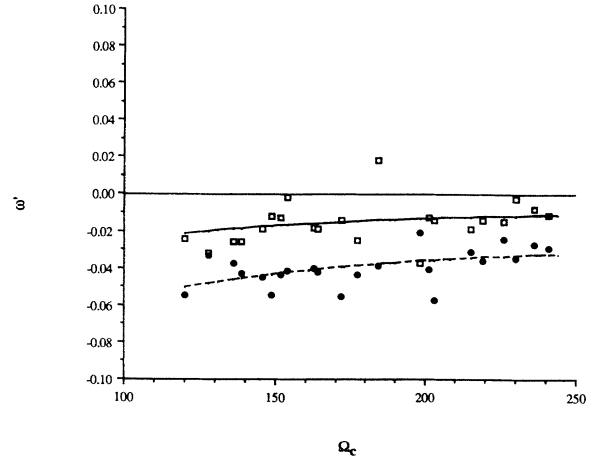

FIG. 7. Dimensionless temporal irregularities' rotation rate with its best fit: □, initial leading edge; ●, initial trailing edge.

leading edge was slower than that of the trailing edge, indicating that the irregularity was becoming smaller in azimuthal length.

An estimate of the time between the occurrence of these irregularities was determined also. The time seems to depend on the shear (the difference between the rotation rates of the cylinders), and, thus, the occurrence time was plotted (Fig. 9) versus the Reynolds number defined by Weisshaar, Busse, and Nagata [15], given by

$$\mathscr{R}=\frac{(\Omega_i-\Omega_o)\frac{1}{2}(R_1+R_2)d}{\nu} . \tag{5}$$

For a given average rotation rate, at low shear rates, the time between occurrences of the irregularity was maximum. At increasing shear rates, this time reached a minimum, and at high shear rates, the time again reached a maximum. It is presumed that at low and high shear rates the time between occurrences would become very large since it corresponds to the edges of the temporal irregularity region of Fig. 4, where they no longer occur.
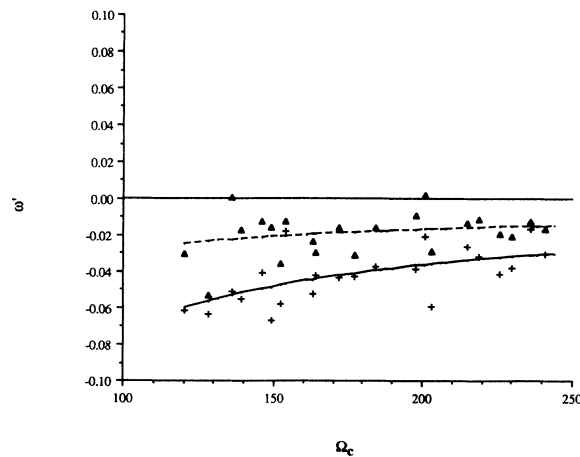

FIG. 8. Dimensionless temporal irregularities' rotation rate with its best fit: +, final leading edge, ▲, final trailing edge.
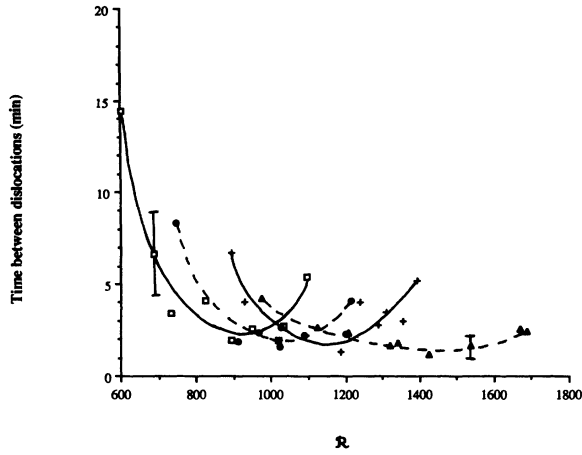
FIG. 9. Time between temporal irregularities: $\square$, $\Omega_C = 120$ to 149; $\bullet$, $\Omega_C = 150$ to 179; $+$, $\Omega_C = 180$ to 209; $\blacktriangle$, $\Omega_C = 210$ to 250.

FIG. 10. $\mathcal{R}/\Omega_C$ versus $\mathcal{R}$ plot of the onset of twists and wavy twists: $\square$, twists; $\triangle$, wavy twists. Also plotted are Andereck's results, $\times$, twists, and $\bigcirc$, wavy twists; and Weisshaar's numerical results for $\gamma = 3.1$, $\blacksquare$, twists, and $\blacktriangle$, wavy twists, and for $\gamma = 2.7$ $+$, twists, and $\bullet$, wavy twists.

4. Twists and wavy twists

A numerical study of the twist vortices was presented by Weisshaar, Busse, and Nagata [15]. A three dimensional perturbation was added to the finite amplitude solutions of the Taylor vortex flow. The onset of twist occurred when the symmetry in the axial direction was broken and azimuthal variations appeared. Curvature effects were neglected by Weisshaar, Busse, and Nagata [15], and the theoretical phase velocity of the twists approached the mean velocity of the cylinders, as observed by Andereck, Dickman, and Swinney [12]. Theoretically, the critical Reynolds number [Eq. (5)] for the onset of the twist vortex flow decreases with increasing axial wavelength. Ordinary twists have a lower critical Reynolds number at low rotation rates, while wavy twists have a lower critical Reynolds number at high rotation rates. In our case, the axial wavenumber γ was fixed (due to the forcing) at 2.743, and is compared with the numerical results of Weisshaar, Busse, and Nagata [15] for $\gamma = 2.74$, as well as for the unforced case, $\gamma = 3.1$. Figure 10 compares the numerical and experimental results for the forced case and for the unforced case of Andereck, Dickman, and Swinney [12]. The trends of the forced and unforced experimental results are similar. The onset of twist and wavy twist decreases with increasing $\Omega_C/\mathcal{R}$. The onset of wavy twists is consistently higher than the onset of twists, for both cases. The onset of the forced twist with the lower axial wave number is lower than the onset of the unforced twist, as predicted by the numerical results. But the onset of the forced wavy twist is higher than the onset of the unforced wavy twist, contrary to the numerical results. This may be due to the fact that, as in the unforced case, the parameters Ω_C and $\mathcal{R}$ do not fully describe the flow. At the moment it is not clear what these parameters might be in the absence of further experiments with different gap widths and forcing wave-
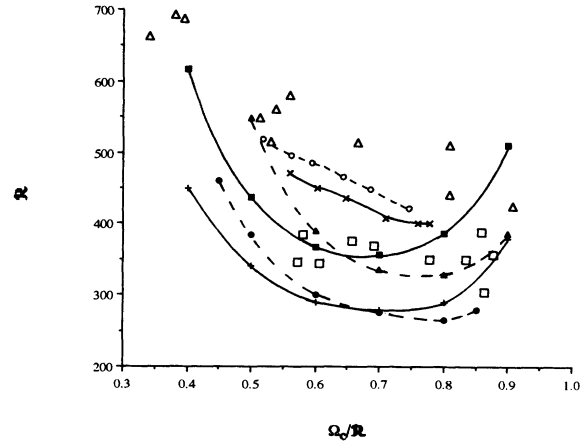
lengths. With either experimental results, the critical $\mathcal{R}$ does not increase at values of $\Omega_C/\mathcal{R} \rightarrow 1$. Also, experimentally, there does not seem to exist a region where the wavy twists have a lower critical value than the straight twists, though the twist and wavy twist results of the experimental forced and unforced cases seem to approach each other as $\Omega_C/\mathcal{R}$ increases.

CONCLUSIONS

Spatial forcing of Taylor vortex flow at an amplitude of 10% of the minimum gap width resulted only in the occurrence of the forced wavelength. This leads to the number of vortex pairs in the system remaining constant. As expected from Chandrasekhar's [2] theory, the appearance of a wavelength 25% greater than the natural wavelength did not affect the onset of Taylor vortex flow. At supercritical rotation rates, most of the flow regimes observed in the unforced case were also observed in the forced case, and they occurred at similar rotation rates. The onset of twists and wavy twists agreed well with the experimental results for the unforced case, but neither of the experiments agreed with the numerical results.

Two new flow regimes were observed. Unstable irregularities occur at low outer and inner cylinder rotation rates. These irregularities occur after the onset of wavy vortices. The amplitude of the wavy vortices seemed to increase until they broke and irregularities occurred. These irregularities occur throughout the tank and were continually changing. In appearance they were similar to the braid vortex flow observed in the unforced case, but this flow moved in solid body rotation with hardly any changes in the dislocations. The other new flow regime

occurred at higher inner and outer cylinder rotation rates, and was named temporal irregularities. These irregularities occurred temporarily and could move vertically and horizontally. The azimuthal rotation rate of these irregularities was found to be proportional to the average speed of the inner and outer cylinder rotation rates.

[1] G. I. Taylor, Philos. Trans. A **223**, 289 (1923).

[2] S. Chandrasekhar, *Hydrodynamic and Hydromagnetic Stability* (Dover, New York, 1961).

[3] S. Kogelman and R. C. DiPrima, Phys. Fluids **13**, 1 (1970).

[4] G. Iooss, J. Fluid Mech. **173**, 273 (1986).

[5] Donald Coles, J. Fluid Mech. **21**, 385 (1965).

[6] H. Riecke, Phys. Rev. A **37**, 636 (1988).

[7] Li Ning, Guenter Ahlers, and David S. Cannell, Phys. Rev. Lett. **64**, 1235 (1990).

[8] P. Matisse and M. Gorman, Phys. Fluids **27**, 759 (1984).

[9] Kwangjai Park, Gerald Crawford, and Russell Donnelly, Phys. Rev. Lett. **47**, 1448 (1981).

[10] Lord Rayleigh, Proc. R. Soc. London, Ser. A **23**, 148 (1916).

[11] E. L. Koschmieder, Phys. Fluids **18**, 499 (1975).

[12] C. D. Andereck, R. Dickman, and H. L. Swinney, Phys. Fluids **26**, 1395 (1983).

[13] C. D. Andereck, S. S. Liu, and H. L. Swinney, J. Fluid Mech. **164**, 155 (1986).

[14] G. W. Baxter and C. D. Andereck, Phys. Rev. Lett. **57**, 3046 (1986).

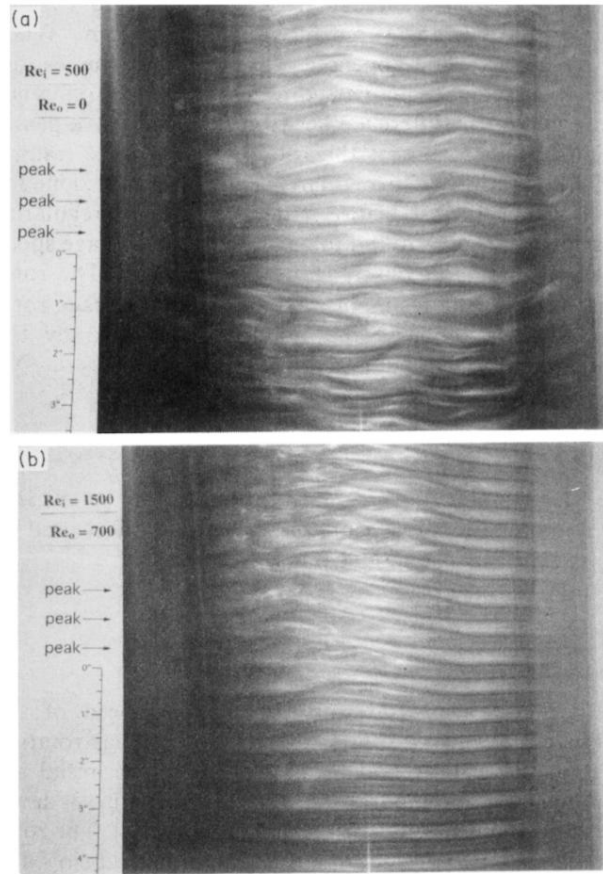[15] E. Weisshaar, F. H. Busse, and M. Nagata, J. Fluid Mech. **226**, 549 (1991).

FIG. 6. (a) Photograph of unstable irregularities. Flow is from left to right. $Re_i = 500$, $Re_o = 0$. (b) Photograph of temporal irregularities. Flow is from left to right. $Re_i = 1500$, $Re_o = 700$.